Aalto University
School of Electrical Engineering
Degree Programme in Micro- and Nanosciences

Kirill Isakov

New nanoporous anti-reflective coating by water treatment of ALD deposited Al_2O_3

Master's Thesis
Espoo, May 23, 2016

Supervisor: Prof. Markku Sopanen
Advisor: M.Sc. (Tech.) Christoffer Kauppinen

Aalto University
School of Electrical Engineering
Degree Programme in Micro- and Nanosciences

ABSTRACT OF
MASTER'S THESIS

Author:	Kirill Isakov		
Title:	New nanoporous anti-reflective coating by water treatment of ALD deposited Al_2O_3		
Date:	May 23, 2016	**Pages:**	v + 44
Major:	Optoelectronics	**Code:**	T-110
Supervisor:	Prof. Markku Sopanen		
Advisor:	M.Sc. (Tech.) Christoffer Kauppinen		

In this work a process for fabricating nanoporous alumina anti-reflective coatings was developed. Anti-reflective coatings were designed for air-glass interface and soda-lime glass was used in the experiments. Alumina was deposited on glass by atomic layer deposition, and then transformed into nanoporous state by immersion in heated de-ionized water.

The conditions for nanoporous alumina creation by de-ionized water treatment were investigated and the resulted structure was analysed with ellipsometry, scanning electron microscopy (SEM), and atomic force microscopy (AFM).

The transmittance of the coated glass was measured in a Cary 7000 spectrometer, showing excellent broadband and omnidirectional performance. The average transmittance for a visible range of spectrum of a double-side coated glass is up to 99.3% versus 91.9% for a non-coated glass. The transmittance for 70° incident light is 85.6% which is 13.9% higher than for pure glass.

Keywords:	nanotechnology, ALD, anti-reflective coatings, alumina, nanoporous materials
Language:	English

Preface

I would like to thank my supervisor Prof. Markku Sopanen for giving me the opportunity to do my Master's Theses in the Optoelectronics group. I wish to thank M.Sc. Christoffer Kauppinen for invaluable guidance, great patience and strong support in my work.

I also want to express my appreciation to D.Sc. Alexander Ch. P. Perros and D.Sc. Ali Shah for profound discussions and helpful ideas. I want to extend my my thanks to Perttu Sippola, Guillaume von Gastrow, Jori Lemettinen and Sami Suihkonen for creating an enjoyable and inspiring working environment.

Together with all, I am respectful to the countless Aalto University teachers for their everyday hard labour which gave me the knowledge to complete this work.

Finally, I am grateful to my parents Liliya Isakova and Andrey Isakov for giving me all the opportunities in life I only wished and their self-giving support to me.

Espoo, May 23, 2016

Kirill Isakov

Abbreviations and acronyms

ARC	Anti-reflective coating
ALD	Atomic layer deposition
DIW	De-ionized water
GPC	Growth per cycle
TMA	Trimethylaluminum
RAE	Rotating-analyser-ellipsometer
QWP	Quarter wave plate
EMT	Effective medium theory
MG	Maxwell-Garnett
EMA	Effective medium approximation
PAA	Porous anodic alumina
PMMA	Poly(methyl methacrylate)
GLAD	Glancing angle deposition
SEM	Scanning electron microscopy
RTP	Rapid thermal processing
RMS	Root mean squared

Contents

Chapter 1

Introduction

Light reflection of glass surfaces is highly undesirable in many applications. It can introduce disturbance into optical lens systems or limit the performance of optoelectronic equipment. Anti-reflective coatings (ARCs) help to overcome these problems by reducing the intensity of the reflected light. Air-glass interface is the most common optical interface within the variety of scientific, industrial or commercial applications. The demand for effective, cheap and easily fabricated ARCs for this interface is only growing. The technology of making ARCs evolves every year bringing new methods of creating them as well as advancing their properties.

ARCs increase transmittance through an optical interface by two main methods: destructive interference and refractive index matching. An index matched coating for the glass-air interface should have refractive index of approximately 1.23. This creates a challenge as there are no inorganic materials with such low refractive index. One of the solutions available in the technology nowadays is creating a nanoporous coating. Introducing porosity into a film decreases its effective refractive index, and if the sizes of the pores are smaller than the wavelength of the light, the light interacts with the film as with a solid medium. ARCs increase transmittance through an optical interface by two main methods: destructive interference and refractive index matching. An index matched coating for the glass-air interface should have refractive in-

dex of approximately 1.23. This creates a challenge as there are no inorganic materials with such low refractive index. One of the solutions available in the technology nowadays is creating a nanoporous coating. Introducing porosity into a film decreases its effective refractive index, and if the sizes of the pores are smaller than the wavelength of the light, the light interacts with the film as with a solid medium.

In this work a new method of creating a nanoporous ARC is presented and the performance of the coating is studied. The fabrication method consists of two steps: atomic layer deposition (ALD) of alumina on glass and immersion of glass samples in heated deionized water (DIW). The DIW treatment introduces porosity into alumina film, which decreases its refractive index to $1.17 - 1.20$.

Chapter 2 of this thesis describes the main features of the ALD technique and principles of reflection reduction used in ARCs, as well as introduces the concept of the effective refractive index, a way to measure it and a short review of nanoporous ARCs. Chapter 3 presents the designed fabrication method of nanoporous alumina ARCs in details. Chapter 4 shows properties of the fabricated ARCs, their performance, and analyses the fabrication method and the results. The summary of the study is presented in chapter 5.

Chapter 2

Background

2.1 Atomic layer deposition

Atomic layer deposition (ALD) is a chemical vapour deposition (CVD) technique, used for depositing thin films with extreme uniformity and thickness control. It is based on consecutive, separated, self-limiting gas-solid reactions. The majority of ALD processes include two reactants sequentially introduced to the reactor and separated by purge steps (flow of nitrogen gas for several seconds) so that excess reactants and by-products are removed before the next reactant pulse. Consequently, ALD process is designed to involve only gas-solid reactions and reactants never meet in the gas-phase [1–4]. The typical binary ALD process includes four following model steps forming a *reaction cycle* which also is illustrated in Figure 2.1:

(1) Self-terminating gas-solid reaction of reactant A.

(2) Purge step to remove excess reactant components and by-products.

(3) Self-terminating gas-solid reaction of reactant B.

(4) Purge step. [1, 2]

The reactants for the ALD process are preferably chosen in such a way that the reactions between them and the surface are brought to saturation within each half-cycle (steps #1 and #3 in Figure 2.1). Such reactions are also called

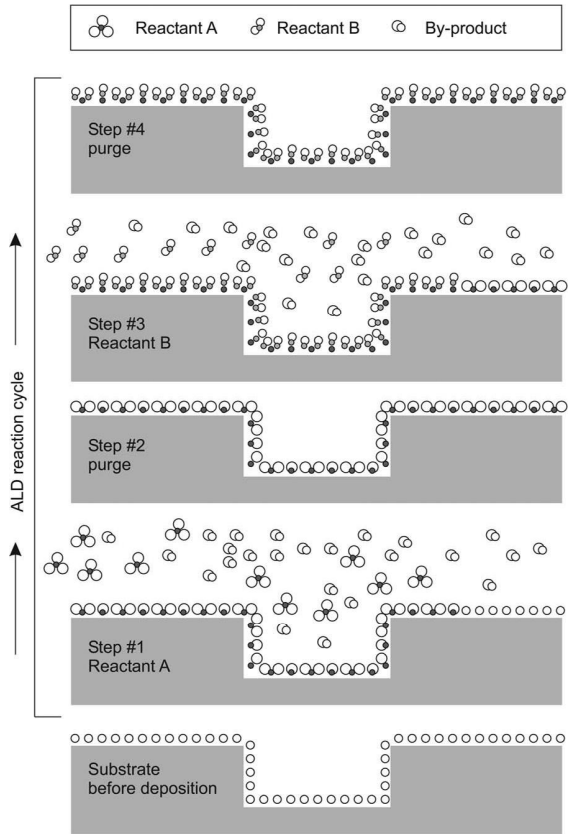

Figure 2.1. Schematic illustration of one ALD reaction cycle. #1 Gas-solid reaction of reactant A. #2 Purge step. #3 Gas-solid reaction of reactant B. #4 Purge step. [1]

self-limiting. The self-limiting nature of the reactions results in fixed growth per cycle (GPC) [1, 2]. A usual GPC for inorganic ALD processes is of the order of few Ångströms which allows a precise thickness control of the film growth [3]. Moreover, as the reactions are brought to completion during each cycle, deposition is not statistical [3] and growth of extremely uniform and smooth films can be achieved.

One of the main advantages of ALD that differentiates it from other film growth techniques is that surface topography only affects the diffusion rate of the reactants [2], but does not affect the uniformity of the film thickness or film quality [6]. Lower diffusion rate increases the time needed for reactants to reach the surface, thus longer cycle times are required. This key feature

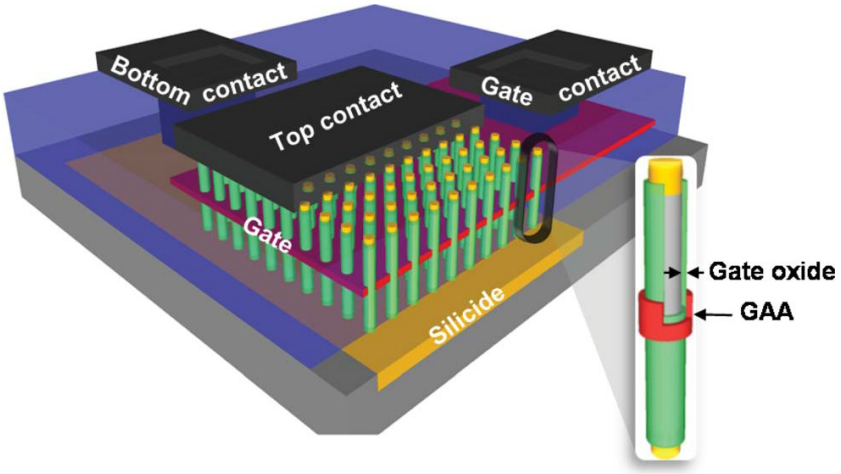

Figure 2.2. Vertical nanowire array-based field effect transistor. [5]

of ALD allows it to conformally (with a constant GPC over any growth direction) coat deep trenches and other demanding 3D nanostructures, such as nanowires (Figure 2.2) [2]. In addition, parallel processing of several large substrates can be performed with high controllability and uniformity [3].

The ALD process is highly dependent on temperature, experiencing significant disruptions in the growth mechanisms with excessively high or low temperature. This results in the formation of a specific temperature range in which the ALD process is both effective in terms of cycle length and gives conformal films [4]. This temperature range is also called *the ALD window* and it typically spans from 100°C to 400°C [2]. Elementary schematic of the ALD temperature window is illustrated in the Figure 2.3. Temperatures lower than the ALD window may not provide enough energy for the reactions to proceed resulting in low GPC. Alternatively, they may not give enough energy for the precursors to escape sufficiently resulting in more GPC, but poor film quality. On the other hand excessively high temperatures result in either decomposition or desorption of the reactants. These limitations restrict the number of possible reactant pairs for a conformal ALD process, or even the possibility to grow certain materials using ALD [2].

Another consequence of the temperature in the ALD processes is the variation of the GPC inside the temperature window. Temperature affects the

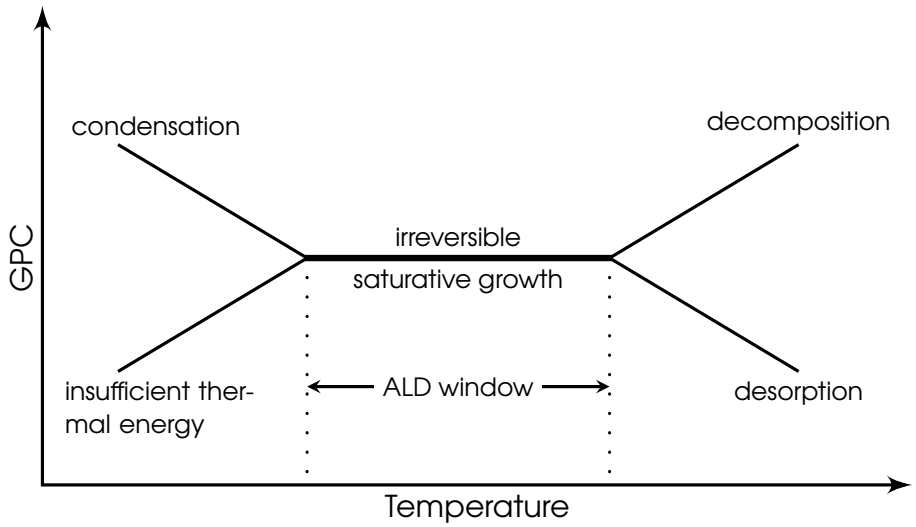

Figure 2.3. Schematic representation of the ALD temperature window. [2]

availability of reactive surface sites, the migration of admolecules (molecules placed above the surface), or may even change the preferred reaction mechanism [2]. This also leads to the fact, that the GPC is usually less than a monolayer thickness of the material growing, due to steric hindrance [7]. Steric hindrance prevents certain chemical reactions to happen as a result of the molecule structure and size, this phenomena is usually observed in molecules with large groups.

The ALD of Al_2O_3 is considered to be a model ALD system and has been continuously used in the semiconductor industry for over two decades [3, 4]. This process is generally implemented using trimethylaluminum (TMA) and H_2O as precursors, and produces amorphous alumina films (a-Al_2O_3). The TMA/H_2O process has close to ideal conditions: the reactants are highly reactive and thermally stable; and as methane is the by-product of the reactions it is pumped out of the chamber and does not disrupt the process [1]. The TMA/H_2O process is described by the formula [1]:

$$2\,Al(CH_3)_3 + 3\,H_2O \longrightarrow Al_2O_3 + 6\,CH_4 \tag{2.1}$$

The reactions between the surface and the precursors correspond to steps

1 and 3 in Figure 2.1 and are described by:

$$\|\mathrm{Al{-}OH} + \mathrm{Al(CH_3)_3} \longrightarrow \|\mathrm{Al{-}O{-}Al(CH_3)_2} + \mathrm{CH_4}, \tag{2.2}$$

and

$$\|\mathrm{Al{-}CH_3} + \mathrm{H_2O} \longrightarrow \|\mathrm{Al{-}OH} + \mathrm{CH_4} \tag{2.3}$$

where symbol $\|$ indicates the surface groups [1, 8].

However, when the ALD process is started on a substrate it can not yet completely follow the described chemical reactions. In case of TMA/H_2O process on silicon substrate-inhibited growth is experienced (for some reactant pairs substrate-enhanced growth may take place). This happens because at first there are less available OH groups on the surface [1], but as the number of performed cycles increases, their concentration grows with the help of the reactants.

2.2 Ellipsometry

Ellipsometry is an old technique (Paul Drude was the first to perform it in 1888) mainly used for measuring properties of thin films such as refractive index and thickness. It is an optical technique which measures the change of the polarization state of light after reflection from the studied surface at non-normal incidence. The obtained data is two independent angles ψ and δ (also known as ellipsometric angles). Ellipsometry provides absolute measurement in a sense that it does not require any reference; however, there is no direct correlation between acquired ellipsometric angles and physical parameters of the sample (thickness and refractive index). Therefore, ellipsometry is a non-direct technique, which always requires the user to create a model (approximate thicknesses and refractive indexes of all the thin film layers in the studied sample in the correct order) in order to perform the measurements.

Ellipsometry is based on the concept of ellipsometric angles. Considering a purely polarized monochromatic wave, the most general polarization of

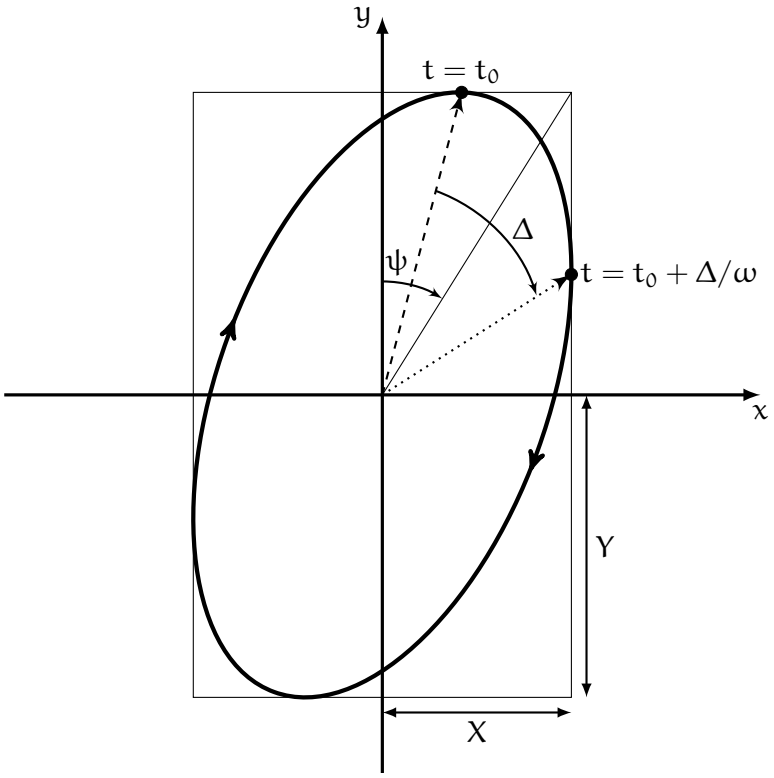

Figure 2.4. Polarization ellipse, described by the ellipsometric angles ψ and Δ. Here $\Delta > 0$ and the polarization is right-handed.

such a wave is elliptic, as linear and circular polarizations are special cases. The projection of the endpoint of the electric-field intensity vector on a plane perpendicular to the direction of propagation of the field is an ellipse as shown in Figure 2.4. The propagation of the wave is assumed to be along the z axis of the right-handed Cartesian coordinate system x-y-z. X and Y denote the amplitudes of the electric field in the x and y directions.

One revolution is achieved in the time interval of $2\pi/\omega$, where ω denotes angular frequency of the light wave. The dashed arrow in Figure 2.4 indicates the the moment when y component reaches its maximum marked as the initial time $t = t_0$. The maximum value of x component is achieved after the time interval Δ/ω (indicated by the dotted arrow). Δ is the *relative phase* of the x and y components of the light wave and it is marked as the angle between dashed and dotted arrows in Figure 2.4. The values of Δ usually vary between $-\pi$ and

π, $\Delta > 0$ denote right-handed polarization and $\Delta < 0$ indicate left-handed one ($\Delta = 0$ means linear polarization).

The value of the angle ψ is related to the relative amplitude

$$\tan \psi = X/Y \, . \tag{2.4}$$

It is usually limited between zero and $\pi/2$.

Ellipsometry is based on measuring the properties of the light wave reflected from the studied sample. The total Fresnel reflection coefficients[1] for parallel and perpendicular polarized components are denoted as r_P and r_S respectively, both of them are complex values. The complex reflectance ratio of the components is given by

$$\rho = \frac{r_P}{r_S} \, . \tag{2.5}$$

Then the fundamental equation of ellipsometry is described as

$$\rho = \tan \psi \, e^{i\Delta} \qquad \text{or} \qquad \tan \psi \, e^{i\Delta} = \frac{r_P}{r_S} \, , \tag{2.6}$$

where ψ and Δ are quantities measured by an ellipsometer.

One of the common structures of an ellipsometer is rotating-analyser ellipsometer (RAE), its scheme is represented on the Figure 2.5. RAE uses a polarizer set to a fixed position, which transforms the unpolarized light from the source to linear polarization. The beam reflected form the sample then passes through the rotating analyser and reaches the detector, where a sinusoidal signal of the light irradiance is collected during one revolution of the analyser. A compensator represented as a quarter wave plate (QWP) can be either placed on the path of the beam or removed from. Installing the QWP changes linear polarized light incident on the sample to a circular polarized one, thus two different sinusoidal signals are scanned during a single measurement:

1. Revolution with the compensator,
2. Revolution without the compensator.

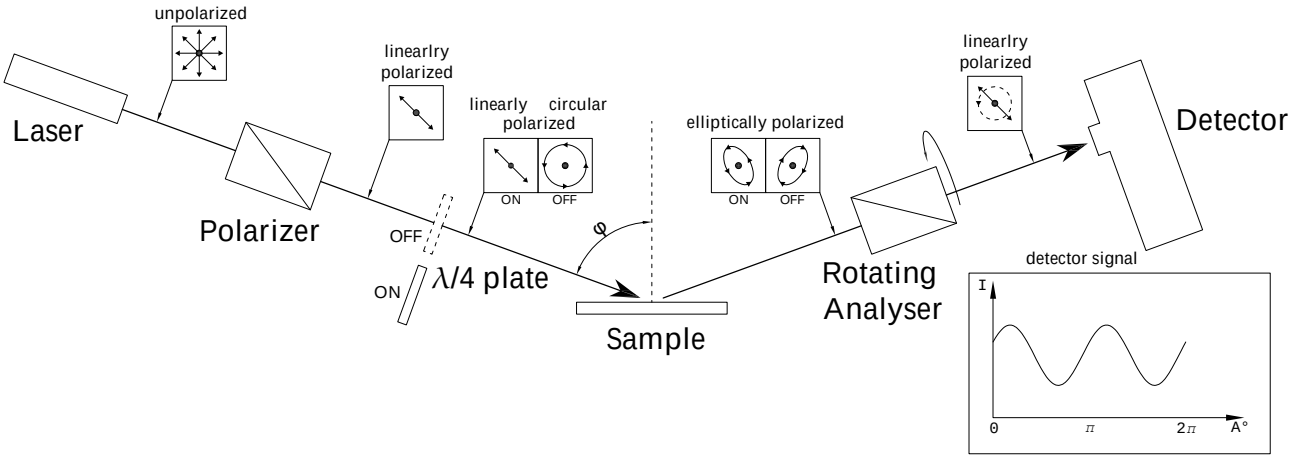

Figure 2.5. Scheme of a rotating-analyzer ellipsometer.

From the obtained irradiance curves cosine and sine Fourier coefficient are calculated which in turn are used to compute ellipsometric angles ψ and Δ. After that user-defined model is used to estimate the thickness, refractive index and absorption coefficient of the thin films on the sample.

2.3 Anti-reflective coatings

Anti-reflective coating (ARC) is a coating deposited on lenses or other optical elements to reduce reflection from their surface. There are two main approaches to achieve reduced reflection: refractive index matching and destructive interference.

2.3.1 Index matching coating

A ray of light crossing an interface of two media with different optical properties experiences reflection. For a plane wave crossing a flat interface of two homogeneous media at normal incidence the radiant intensity of reflected light

[1]The concept of the Fresnel reflection coefficients will not be described in this Master's theses. The Reader can familiarize himself with this by reading *Optical physics* by Lipson et al. [9].

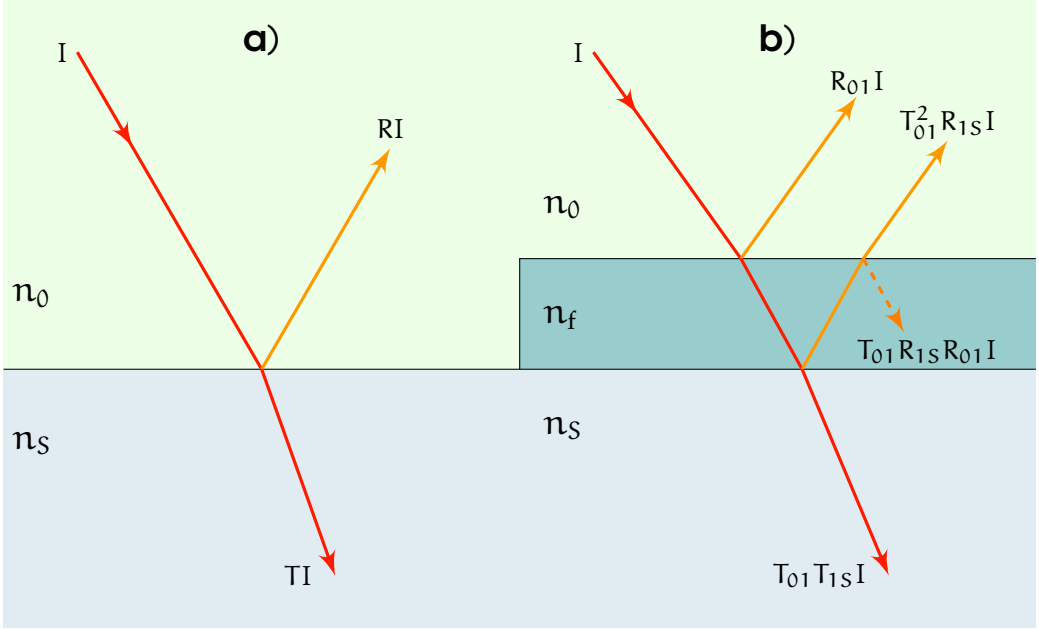

Figure 2.6. Reflection and transmission at the interface of **a)** two media and **b)** three media.

is given by *reflectance*

$$R = \left(\frac{n_0 - n_S}{n_0 + n_S}\right)^2 , \tag{2.7}$$

where n_0 and n_S are the refractive indices of the first and the second media, respectively.

Transmittance represents the intensity of the transmitted light, for the case when absorption and scattering are neglected (usual scenario for most homogeneous transparent materials)

$$T = 1 - R . \tag{2.8}$$

Consequently, for a beam of light with intensity I crossing an interface of two media a beam of intensity RI is reflected and a beam of intensity TI is transmitted into the second medium (see Figure 2.6a).

The reflection can be reduced by introducing a film with a refractive index of n_f so that $n_0 < n_1 < n_S$ as shown in Figure 2.6b.[2] The total transmittance in

[2]There are multiple reflections inside the film, but their amplitudes are small and they can be neglected.

this case is described as

$$T_{total} \approx T_{01} T_{1S} \, . \tag{2.9}$$

As $T_{01} = 1 - R_{01}$ and $T_{1S} = 1 - R_{1S}$ the equation for total transmittance transforms into

$$T_{total} = \frac{16\, n_0\, n_f^2\, n_S}{(n_0 + n_f)^2\, (n_f + n_S)^2} \, . \tag{2.10}$$

The total transmittance can be examined as a function of the refractive index of the introduced film n_f. Hence the optimum value of n_f which maximizes the total transmittance can be found. The computations for this are quite cumbersome and will not be shown here, but the optimum value is given by the geometric mean of the surrounding indices:

$$n_f = \sqrt{n_0 n_S} \, . \tag{2.11}$$

Note that at this value reflectances at the first and second interfaces are equal.

This approach is called index matching. For the interface of air $n_0 \approx 1$ and soda-lime glass $n_S = 1.52$ the optimum refractive index for the coating is $n_f = 1.23$. Introducing such a coating increases transmission from ~96% to ~98% (at a single air–glass interface). The problem is that there are no inorganic materials with such low refractive index [10]. Porosity can be introduced into a medium to artificially lower the effective refractive index[3].

The term *effective refractive index* is applied to heterogeneous materials which interact with light like a homogeneous material with new optical properties. This occurs when the sizes of the features in the heterostructure are smaller than the wavelength of the incident light. Hence, the light does not refract from these features but behaves like it is propagating through a medium with some certain effective refractive index. A surface structured material can be observed as a heterostructure of the material itself and air.

2.3.2 Destructive interference coating

When a light beam propagates through the boundary of two media separated by a thin film coating two reflected waves are generated at the two interfaces:

[3]The concept of nanoporous materials is described in the Section 2.4

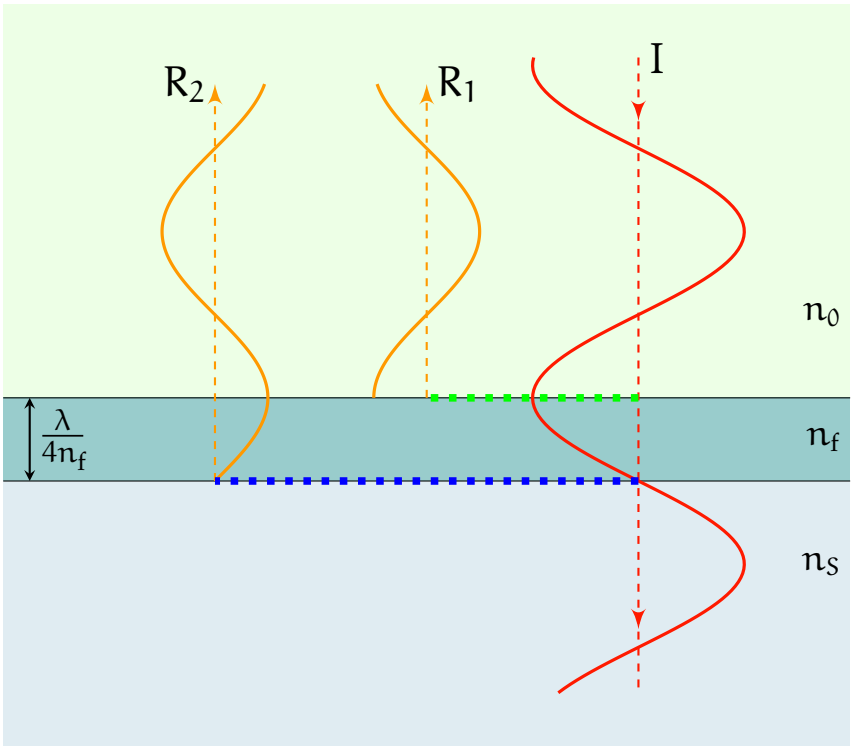

Figure 2.7. Schematic representation of destructive interference in a quarter-wave anti-reflection coating.

the first medium – coating and coating – the second medium. These waves interfere with each other and this feature can be utilized to further decrease reflection by adjusting the thickness of the film to satisfy the conditions for destructive interference.

Destructive interference occurs when the two reflected waves have a phase shift of π between each other as shown in Figure 2.7. In order to achieve this a precise control of the film thickness is needed. In the case of normal incidence the wave R_1 is shifted to the wave R_2 by the value

$$\phi = \frac{2\pi n_f L}{\lambda} = \frac{4\pi n_f d}{\lambda}, \tag{2.12}$$

where $n_f L = 2n_f d$ is the optical path difference between the beams, λ is the vacuum wavelength, d is the thickness of the film and n_f is its refractive index. This phase shift occurs due to longer path of the second reflected beam, as it goes through the film twice before getting out of it and meeting the first

reflected beam. Since for destructive interference $\phi = \pi$ the film thickness must be:

$$d = \frac{\lambda}{4\, n_f} \tag{2.13}$$

A film of such thickness is also called *quarter-wave coating*.

As seen from Equation 2.13, destructive interference strongly depends on the wavelength of the incident light. Nevertheless, if the phase shift does not perfectly satisfy Equation 2.12, but is close to the desired value, then the anti-reflective properties of the film only decrease somewhat and do not disappear completely. Therefore, achieving destructive interference at single wavelength decreases reflection at nearby wavelengths as well. In addition, at non-normal incidence the phase-shift between two reflected beams increases, though the reflection will still be decreased by the film.

Also note that as seen from Figure 2.6b the second reflected beam has different intensity (hence amplitude) than the first one, which appears to be slightly smaller due to the factor T_{01}^2 (considering index matched coating where $R_{01} = R_{1S}$). This means that in practice quarter-wave coating can not completely annihilate reflection even at single wavelength, although it can reduce it dramatically.

2.4 Nanoporous materials as ARCs

As was mentioned in Subsection 2.3.1, there are no inorganic materials with refractive index of 1.23, which would satisfy the conditions for index matching coating for the glass-air interface. However, the effective refractive index can be reduced by introducing porosity into a solid medium.

2.4.1 Effective Medium Theory

Nanoporous material can be represented as a mixture of a solid medium and voids (usually filled with air air) called pores. The refractive index of such a material depends on its topology [11]. As long as the pores are small enough

so they do not cause a light scattering, *effective medium theory* (EMT) can be used for calculations [12]. According to EMT, a random unit cell of a nanoporous material can be exchanged with a homogeneous medium so that the optical properties of the structure remain unchanged. The refractive index of such medium is replaced by effective refractive index, [12] which can be calculated by various mathematical models. The two most common ones are Maxwell-Garnett (MG) model and Bruggeman effective medium approximation (EMA). While both of them are applied to a situation when a nanostructure consist of two materials, MG model treats one of the materials as the host and the other as inclusions unlike the EMA, which treats both materials on an equal basis. Because nanoporous ARCs usually have a large volume fraction of pores, EMA is suggested to be used as it is physically more appealing in such a scenario and was favoured by data collected in ellipsometric measurements of effective refractive index [13].

Bruggeman's approximation can be presented as [11–14]

$$f_1 \left[\frac{n_1^2 - n_{\text{eff}}^2}{n_1^2 + 2n_{\text{eff}}^2} \right] + f_2 \left[\frac{n_2^2 - n_{\text{eff}}^2}{n_2^2 + 2n_{\text{eff}}^2} \right] = 0 \,, \tag{2.14}$$

where n_1 and n_2 are the refractive indexes of the two media (e.g. solid material with pores filled by air), f_1 and f_2 are their volume fractions respectively, n_{eff} is the effective refractive index of the structure.

Note that $f_2 = 1 - f_1$, hence for a nanoporous structure with pores filled by air, it is possible to calculate the volume fraction of the pores if the effective refractive index of the structure and refractive index of the solid are known.

The size of the features in nanoporous material influences the applicability of EMA. Thus for the wavelength of 400 nm and the volume fraction of the pores of 0.5 an error of 1% is expected in calculations of the effective refractive index at the 7 nm pore radius; the pore radius of about 20 nm leads to an error of 10% [12]. For longer wavelengths the EMA is valid up to larger limiting radii.

Another method to calculate the effective refractive index of porous mate-

rial relies on the relation [10, 11, 15]

$$\frac{n_p^2 - 1}{n^2 - 1} = \frac{d_p}{d}\,, \tag{2.15}$$

where n and d are refractive index and density of the as-deposited material, and n_p and d_p are refractive index and density of the porous material (note: n_p is the same as n_{eff} used previously), respectively.

Now Equation 2.15 can be expressed in terms of porosity [10, 11, 15]

$$\frac{n_p^2 - 1}{n^2 - 1} = 1 - \frac{P}{100}\,, \tag{2.16}$$

where P is percent porosity, which reflects the volume fraction of the pores in the material.

2.4.2 Examples of nanoporous ARCs

In this section some examples of nanoporous ARCs on glass substrates are given.

Formation of porous oxide from a sol-gel

In 1970s–80s Bulent E. Yoldas proposed methods to form porous Al_2O_3 films from sol-gels [10, 16, 17]. In general the method can be described as[4]

1. Preparation of aqueous solution from Al alkoxides.
2. Peptization of the solution with an acid.
3. Dehydration of the solution to form a gel (e.g. by boiling).
4. Deposition of the gel onto a substrate (e.g. by dip coating).
5. Baking of the coating (temperatures: 450–500°C) and formation of the porous Al_2O_3 film. [10, 17]

[4]The encountered chemical terms will not be explained in this work, as the description of this process is not the essential part of the work.

The ARCs obtained by Bulent E. Yoldas in 1980 [10] had porosity of ~64% with the average pore radius of 40 Å. The refractive index in the bulk material was ~1.296, while the lowest refractive index in coatings with the thickness of ~0.1 µm was 1.318. The coatings showed minimum reflectance of 1.4% for about 600 nm light, the reflectance increased for lower or higher wavelengths.

Porous anodic Al_2O_3

In 2012 Junwu Chen [18] described a method capable of creating graded-index porous anodic alumina (PAA) coatings. The technique of making the coating consists of four general steps:

1. Deposition of pure Al films by electron-beam evaporation.
2. Anodization of Al film in oxalic solutions and formation of PAA.
3. Immersion of the film in H_3PO_4 solutions to enlarge the pore diameter.
4. Annealing of the sample in air at 550°C. [18]

The diameter of pores and so the refractive index is controlled by time of the immersion in the acid. The graded-index profile was implemented by consequently repeating steps 2 and 3, creating layers with different refractive indicies in a top-down manner. [18]

The lowest refractive index obtained was $n = 1.08$ with the pore diameter of 40 nm. The non-etched PAA had $n = 1.47$ which allowed the whole window from 1.08 to 1.47 to be used for creating graded-index profile of the film. The profile was successfully created with five layers of PAA arranged in Gaussian manner in respect to refractive index. As the result the lowest reflectance of 0.64% at the wavelength of 534 nm was achieved. Overall reflectance in the visible range of light spectra was about 1–2% with the peaks up to 3%, while the reflectance of uncoated glass was 8.37%. The angular performance of the coating was measured as well, showing efficient improvement only for TE polarized mode decreasing reflectance from ~50% to ~30% at 80° incident angle. [18]

Spin casted polymers

The first ARC prepared by spin casting a polymer latex was reported by Hao Jiang et al. [19] in 2007. In that work transmittance of 95.7% at 550 nm for a single-side coating and 99.5% for a double-side coating on glass was achieved. The coating was prepared from a poly(methyl methacrylate) (PMMA) particles.

In 2010 Xiao Li et al. [20] developed a process of creating a gradient refractive index structure by spin casting the solution of a polystyrene-block-poly(methyl methacrylate) (PS-b-PMMA)/(PMMA) blend onto an octadecyltrichlorosilane[5] (ODTS)-modified glass substrate. The resulting ARC showed the transmittance of >97% for visible and near-infrared light. In addition, remarkable performance at high incident angles was achieved: 94.8% transmittance at 60° incidence of light for a double-side coated glass.

Glancing (oblique) angle deposition

Another approach for the fabricating of porous ARCs is glancing angle deposition (GLAD). GLAD is an improved physical vapour deposition technique: a vaporized material condenses onto a rotating substrate with the vapour flux incident at an angle. [11]

High incident angles of the vapour flux induce atomic shadowing in the grown film providing columnar growth [11, 21]. By alternating the incident angle or the rotation speed of the substrate the porosity of the grown film can be modified, and thus, its refractive index can be controlled. The control over the film microstructure is highly accurate and graded density with a Gaussian profile was obtained by Scott R. Kennedy and Michael J. Brett in 2003 [22]. Their anti-reflective coatings on glass showed peak transmittance up to 99.9%, while having transmittance over 99.7% with the bandwidth greater than 460 nm covering most of the visible spectrum.

[5] $CH_3(CH_2)_{17}SiCl_3$

Chapter 3

Experimental details

The developed process of creating the porous alumina anti-reflective coating will be described in this chapter. Section 3.1 contains the details about the deposition of Al_2O_3 by ALD. Section 3.2 describes the post processing of the ALD alumina with water to introduce porosity in the film.

The films were prepared on pairs of glass and Si samples, as a sufficient way to perform ellipsometric measurements on a transparent substrate was not possible (the intensity of a beam reflected from a transparent sample is the sensitivity of the ellipsometric tool is not sufficient). Consequently, the thickness of the porous film and its effective refractive index were obtained from the Si samples and transmittance was measured from the glass samples.

All the fabrication was conducted in the Micronova cleanroom.

3.1 Atomic layer deposition recipe and details

Atomic layer deposition was carried out by using a thermal ALD reactor manufactured by Beneq (model name TFS 500). A planar reaction chamber was used for processing Si wafers and glass pieces. The schematic of the ALD reactor and its reaction chamber is illustrated in Figure 3.1.

The deposition of Al_2O_3 was carried out on four-inch Si (100) wafers and

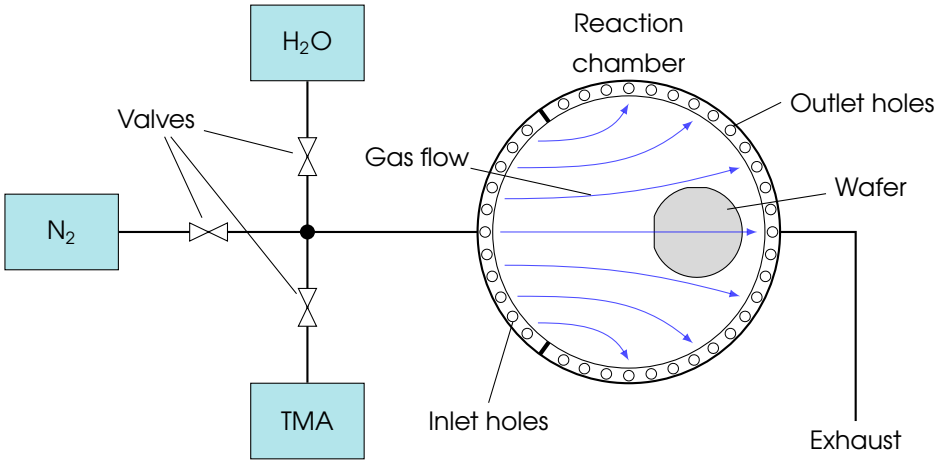

Figure 3.1. Schematic of the ALD reactor used for the Al_2O_3 deposition and the placement of the wafer in the reaction chamber.

glass slides[1] (during the ALD the glass slides were placed on a six-inch dummy wafer to suppress the film deposition on their back sides). Note the correct placement of the wafer in the reaction chamber represented in the Figure 3.1. This is important as the further the wafer is from the inlet holes, the more uniform gas flow passes along its surface and the better is the uniformity of the deposited film.

The used precursors, as described in Section 2.1, were TMA and H_2O as this is the standard Al_2O_3 ALD process. The reaction cycles consisted of the following steps (flows):

- 200 ms TMA,
- 750 ms wait,
- 1 s N_2 (purge),
- 200 ms H_2O,
- 1 s wait,
- 1 s N_2 (purge).

The total cycle time is 4.45 s. This recipe has proven to have the shortest cycle time yet bringing the reactions into saturation (for the used setup and tool).

[1]Detailed information about the used glass is given in Appendix A.

The deposition of alumina for ARC was performed at the temperature of 120°C, as this is the lowest available temperature within ALD temperature window for the standard Al_2O_3 recipe. This choice is justified by the fact that at lower temperatures the level of amorphousness and disorder is higher in the deposited film, and this feature benefits the post processing with water which introduces porosity.

The deposition targeted the thickness of 28 nm. The growth rate at 120°C with the used recipe was measured in advance, showing 0.9 Å per cycle, consequently 313 cycles was performed to get the desired thickness. The choice of the thickness is explained by the fact that introducing porosity into alumina by the water treatment (Section 3.2) significantly increases the film thickness. Consequently, the films after the treatment had thicknesses of 120 nm – 140 nm, which satisfies the conditions for destructive interference for 550 nm – 650 nm wavelengths, according to Equation 2.13.

Before deposition the standard RCA-1[2] cleaning process and the subsequent oxide strip by 50% hydrofluoric acid was carried out on the silicon wafers. After that Si was let to grow natural oxide for several days in a sealed box with ambient atmosphere. The glass slides were cleaned with acetone, isopropanol and rinsed with deionized water (DIW).

The substrate-enhanced or -inhibited growth effects on glass and silicon wafers were not measured, but were assumed to have negligible difference as the wafers had natural SiO_2 layer before the deposition and the glass itself consists of oxides, 73% of which is silica.

Alumina films were grown by ALD under other conditions in order to check if the DIW treatment would take the same effect on them. Thus Al_2O_3 films were created in the same tool at 300°C and in another Beneq TFS-500 reactor also at 300°C, but with slightly different recipe.

[2]RCA-1 procedure removes organic residues and particles. The process represents soaking the wafers in 80°C solution of $H_2O_2 : NH_3 : H_2O$ for 10 minutes. The recipe for the solution: 5 parts of deionised water, 1 part of 25% ammonia, 1 part of 30% hydrogen peroxide.

3.2 Water treatment

Crystalline Al_2O_3 is insoluble in water and is proven not to be affected by it in any way. However, an amorphous Al_2O_3 film deposited by ALD is corroded by water [23, 24]. In this research the possibility of transforming ALD alumina into nanoporous state is presented (more discussions on this phenomena in Chapter 4).

The pairs of alumina coated Si and glass samples were put into heated deionized water of constant temperature for 30 minutes. A heating bath manufactured by IKA (model name HBR4) was used for the temperature control. Different DIW temperatures from 20°C to 90°C were tested. With sufficiently high DIW temperature the surface of the alumina film was roughened which was observed by eyes as an increase in hydrophilic properties of the film and significant increase in scattering of a reflected laser beam (in the ellipsometry set-up).

The DIW acts not only on the surface of the film, but also penetrates into it, so that volume interaction occurs. However, the depth of this processing is limited, and thick films can not be completely processed. A 100 nm thick sample was treated with DIW and had lower porosity at the bottom, than at the top. The study of the exact value of the maximum film thickness available for the DIW treatment was not performed in this work.

The samples prepared at 300°C and in the other ALD reactor were immersed in the heated DIW. There were no noticeable differences in the results of the treatment, films deposited at higher temperatures were also transferred into a porous state.

Chapter 4

Results and analysis

4.1 The ellipsometric measurements

The thicknesses of the Al_2O_3 films deposited on Si were measured two times – after the ALD deposition and after the DIW treatment – by the ellipsometer Plasmos SD2300. To provide the exact data, the measurement results are given in Table 4.1 together with the temperature of the DIW treatment. For a better analysis, Figure 4.1 shows how the processing increased the thickness of the alumina film due to introduced porosity and the resulting effective refractive index depending on the DIW temperature.

As can be seen from Figure 4.1, there is a specific temperature of about 50°C after which a significant increase in the film thickness is observed as well as a substantial drop in the effective refractive index. This *critical temperature* (T_{cr}) is mostly tied to the chosen immersion time (30 minutes), but also depends on the used ALD recipe for the deposition of the Al_2O_3 film. Based on this data the following assumption was made: with the increase of temperature amorphous alumina reaches certain energy when the process of its reorganization starts, which is both conducted and catalysed by water. It was also assumed, that the minimum temperature for the reorganization to start is rather low, and in practice temperature mostly affects the speed of the process in an Ar-

№	As deposited		T, °C	Porous	
	n_{dep}	d_{dep}, Å		n_{por}	d_{por}, Å
1	1.641	277	19.4	1.643	272
2	1.645	275	38.4	1.642	273
3	1.641	275	40.0	1.643	276
4	1.640	277	44.2	1.454	370
5	1.639	280	48.2	1.446	394
6	1.641	276	50.4	1.177	1425
7	1.643	278	52.1	1.168	1404
8	1.642	279	60.5	1.186	1350
9	1.642	275	70.1	1.199	1255
10	1.644	274	80.8	1.201	1231
11	1.643	279	90.5	1.204	1214

Table 4.1. Ellipsometric measurements before and after the water treatment, and temperature of the water treatment. Here n_{dep} and d_{dep} are the refractive index and the thickness of the as-deposited Al_2O_3 film, n_{por} and d_{por} are the index and the thickness of the treated porous film, respectively.

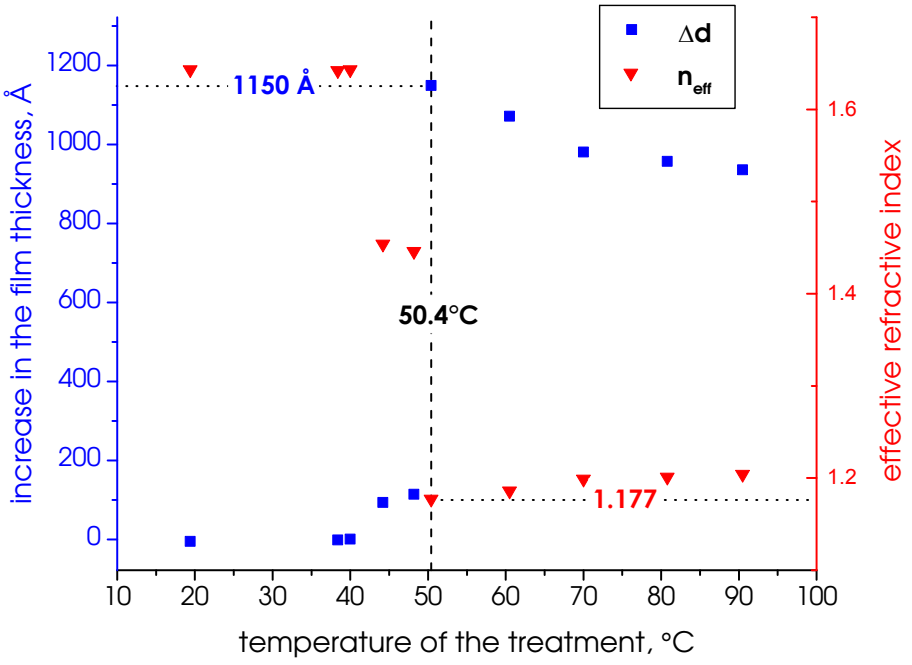

Figure 4.1. Effective refractive index (n_{eff}) and extension of the thickness (Δd) of the porous alumina film vs. water temperature.

rhenian manner[1]. However, the reorganization of the alumina saturates after reaching a certain maximum porosity level, associated with the least dense structure the film can have. Combining the Arrhenian temperature influence on the reorganization process and the self-saturation of the process gives a curve of the similar shape to the refractive index curve in Figure 4.1.

The lowest achieved effective refractive index ($n = 1.168$) is also observed near the critical temperature, whereas the higher temperatures results in higher n_{eff} and lower increase in thickness. This phenomenon can have several possible origins. One of them is that higher treatment temperatures result in more dense packing of the reorganized structure, as there is more energy available to find a more beneficial organization. Another potential reason is that the optical properties of the alumina itself change at higher temperatures of the treatment and, consequently, the properties of the whole structure change as well (although, the change in the atomic structure of the Al_2O_3 is unlikely to happen at such low temperatures, e.g., crystallization of alumina takes place at above 1000°C [25]). The lower thickness increase can also originate from the loss of Al_2O_3 in water (it was not clear if any of alumina dissolves in water during the process).

The calculations of the porosity level were conducted by three methods: according to the Bruggeman's approximation (Equation 2.14), by the Bulent E. Yoldas's formula (Equation 2.16), and from the ratio of the as-deposited film thickness and porous film thickness:

$$f_{air} = 1 - \frac{d_{dep}}{d_{por}} \, . \tag{4.1}$$

However, as there probably is some loss of the material during the DIW treatment of Al_2O_3, this formula will have some error with the real porosity of the material, but it can be used for an approximate estimation as well.

The dependence of the porosity level (calculated by the three methods) of the alumina films on the temperature of the DIW treatment is given in Figure 4.2. The results from the different methods differ, which indicates that the

[1] $f(x) = Ae^{-B/x}$, where A and B are constants. This function has exponential behaviour at first, then it levels off as it approaches the limit.

assumptions required for using them are not completely met. Nevertheless, they give a rough notion of the porosity level in the DIW treated ALD alumina films. In addition, all the three methods identically describe the qualitative changes in the porosity of the films: the shapes of the curves are similar.

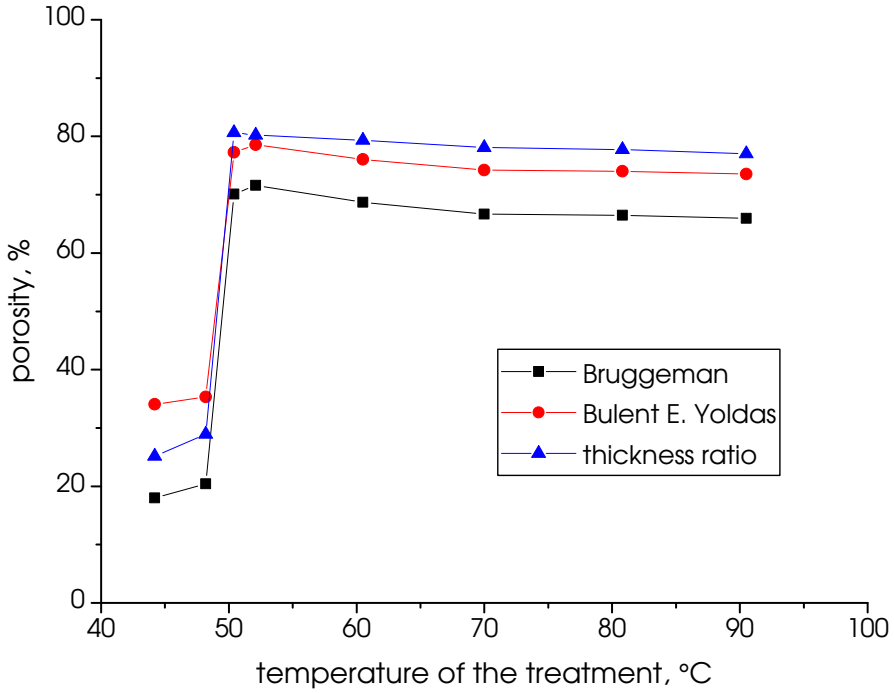

Figure 4.2. The porosity of the treated Al_2O_3 film calculated by 3 different methods: Bruggeman approximation, Bulent E. Yoldas's formula, and the film thickness ratio.

Reliability of the ellipsometric measurements

The reliability of the ellipsometric measurements of the porous Al_2O_3 films was questioned; thus, the thickness of an additional sample was checked by measuring the step height of the film with a profilometer (Dektak XT manufactured by Bruker). In order to do that a part of the film was protected with a resist while the unprotected alumina was etched away with a H_3PO_4:HNO_3 solution. The step height measured by the profilometer and the film thickness acquired from the ellipsometry differed for less than 10%. Such a difference

may have originated from the effects of isotropic etching or resist deposition on the porous film, so the ellipsometric measurements were considered reliable.

4.2 Scanning electron microscopy and roughness

In this section scanning electron microscopy (SEM) images of the porous Al_2O_3 films fabricated at various conditions are provided. All the images except the cross-sectional image are taken from approximately 20° angle to the film surface. The samples for SEM were prepared on Si substrates.

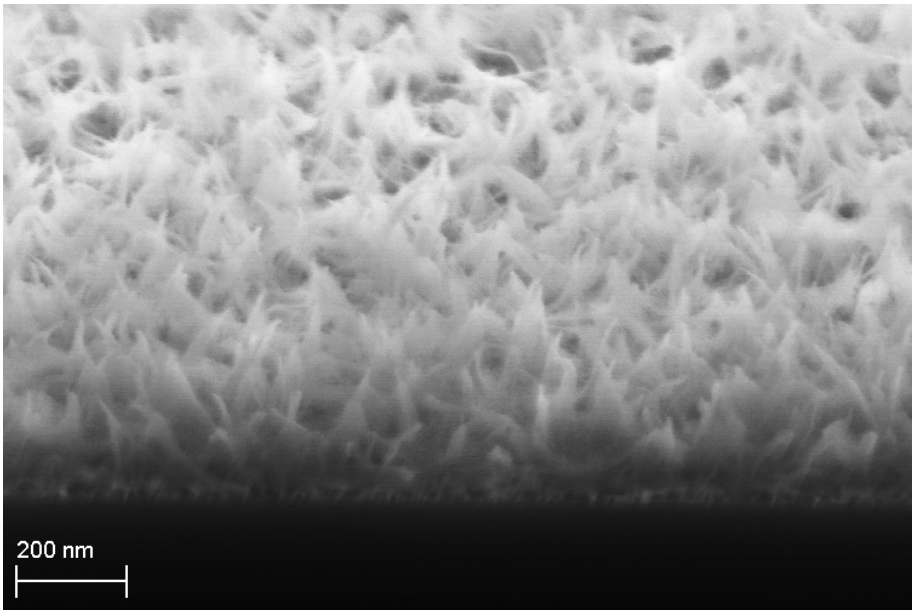

Figure 4.3. SEM image of a porous alumina film taken from ca. 20° angle to the surface of the film. At the bottom of the picture is the Si substrate, which appears black.

Figure 4.3 shows that the porous alumina film has grass-like structure and the surface has high roughness. From the cross-sectional view (which was taken almost parallel to the surface of the film) shown in Figure 4.4 it can be seen that the density of the film has a gradient, it increases closer to the substrate.

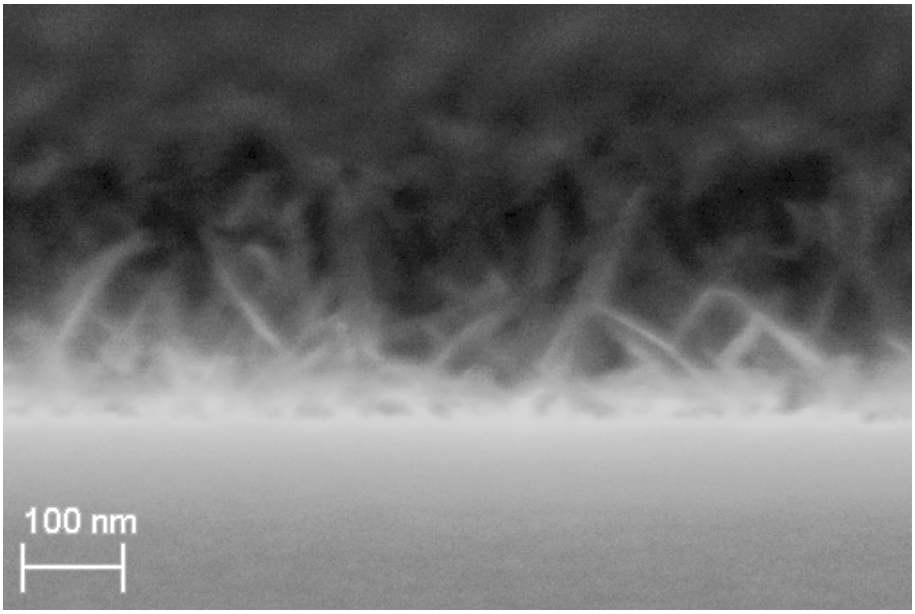

Figure 4.4. Cross-sectional view of a porous alumina film taken approximately parallel to the film surface. Si substrate can be seen at the bottom.

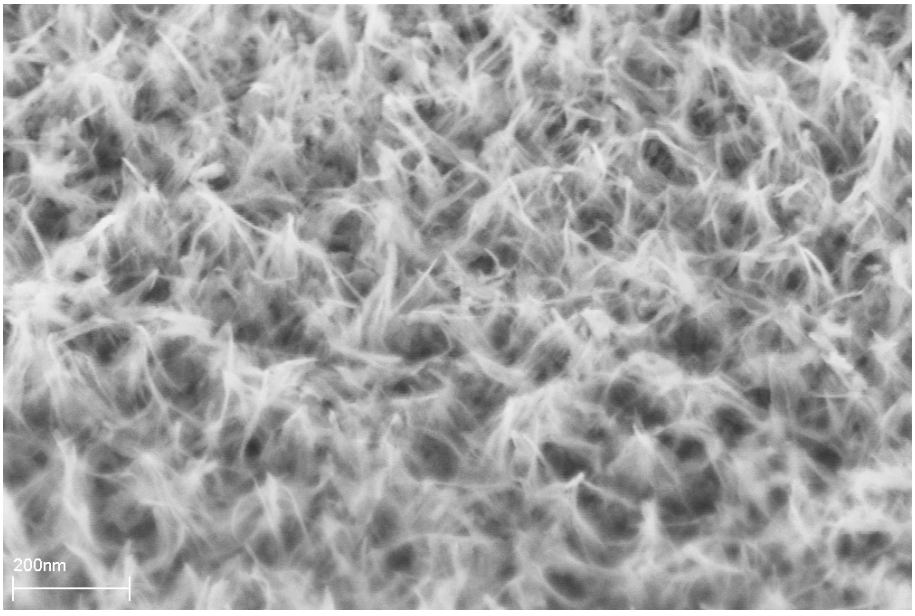

Figure 4.5. Porous alumina film annealed by RTP in N_2 for 5 min at 950°C. Higher contrast of the picture is achieved by the annealing.

Overall, the structure consists of *fibres* or *flakes* of Al_2O_3 separated by voids. The sizes of the features in the material span from ca. 1 nm to 10 nm in the "bulk" of the porous alumina, but on the surface the gaps between the peaks are significantly larger: up to 100 nm. This increases scattering of the reflected light and explains the clear visibility of a laser beam hitting the surface during the ellipsometric measurements (unlike the as-deposited Al_2O_3).

One of the porous Al_2O_3 films was annealed by rapid thermal processing (RTP) for 5 minutes in nitrogen atmosphere at 950°C, and a SEM image from it is presented in Figure 4.5. The picture appears to have much higher contrast and the grass-like structure of the film can be seen more clearly. The increase in the contrast is related to the increase in the conductivity of the Al_2O_3 after annealing as the precursor residuals like carbon and hydrogen diffuse out of the film during annealing . Higher conductivity means better transfer of the electrons to the substrate during the SEM (charging of the surface decreases). However, annealing did not give significant changes in the optical properties of the films and was not used for the producing of the ARCs.

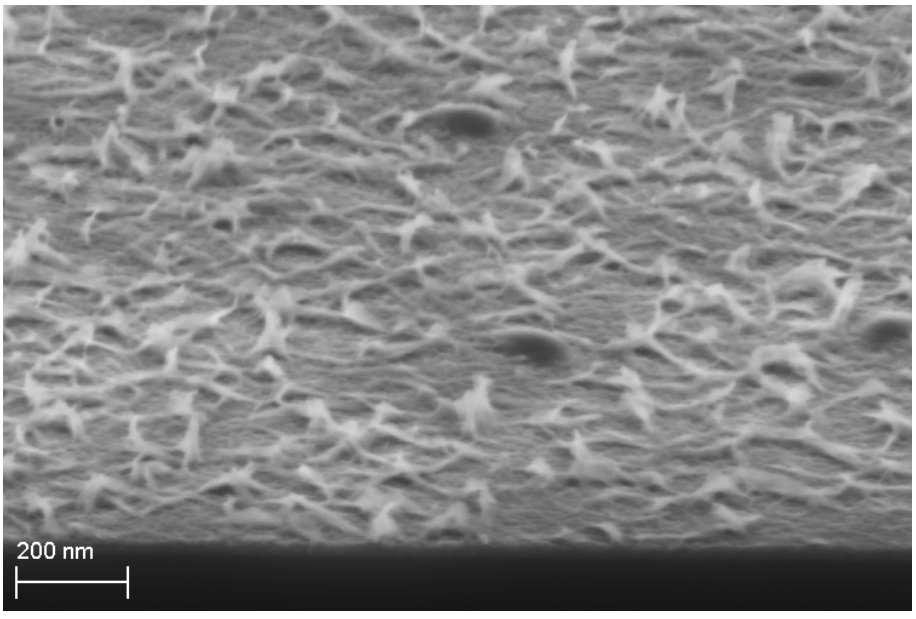

Figure 4.6. The surface of the Al_2O_3 immersed in DIW at 46°C for 30 minutes.

The surface of the alumina film treated at 46°C in DIW is presented in

Figure 4.6. This temperature is close to the T_{cr} for the 30 min process as shown in Figure 4.1 and the resulting refractive index of the alumina film is ca. 1.45. It can be clearly seen that only the surface of the alumina is affected by the treatment, but there are no significant transformations in the bulk of the film. The peaks on the surface are organized from the *flakes* of the Al_2O_3 taken out from the bulk.

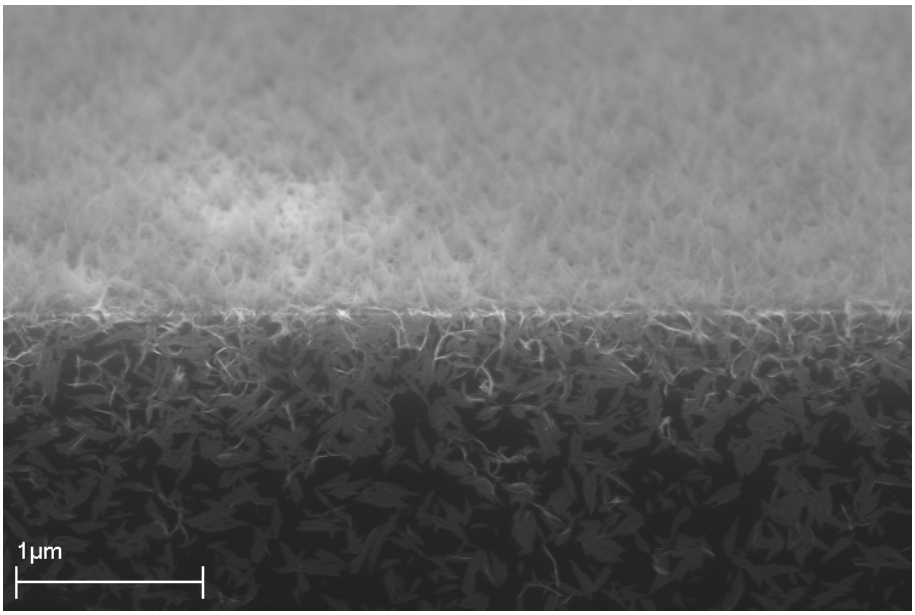

Figure 4.7. Flakes of alumina on a side of the silicon substrate cleaved before the DIW treatment of Al_2O_3.

Figure 4.7 shows a side of the Si substrate after the DIW processing of alumina. Some flakes of Al_2O_3 can be clearly seen to be transferred to the side of the silicon substrate. This means that some pieces of the material are completely taken out from the bulk. It also leads to the conclusion that there must be some loss of the material during the treatment.

The demonstrated SEM images show that the surface roughness of the alumina coatings changes with the temperature of the DIW treatment. The root mean squared (RMS) roughness [2] was measured by an AFM (Dimension 3100

[2]RMS roughness is calculated by the formula: $R_{RMS} = \sqrt{\frac{1}{n}\sum_{i=1}^{n} y_i^2}$, where y_i - height of

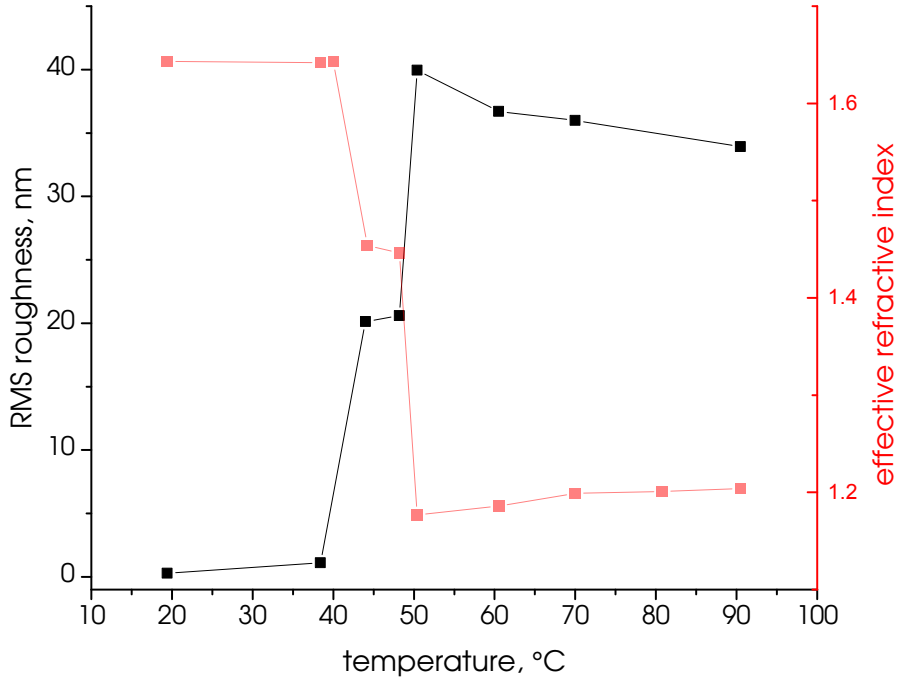

Figure 4.8. RMS roughness of the alumina coatings depending on the temperature of the DIW treatment comparing to the effective refractive index of the coatings.

manufactured by Digital Instruments). Figure 4.8 presents the obtained values. There is a strong correlation in the surface roughness and the effective refractive index of the films as can be seen from the figure. The roughness increases significantly with a certain critical temperature. However, the increase in the roughness starts earlier than in the refractive index. This phenomenon is explained by the fact that the DIW treatment first affects the surface of the film and not the bulk of the material. Changes in only the surface do not lead to significant changes in the optical properties of the coatings.

---

the topological feature measured at a point, n - number of the measurement points.

4.3 Understanding the process

It was not clear what processes occur in the amorphous ALD alumina during the immersions to the heated DIW, and how the film is transformed into a porous state. The process as observed from the SEM images can be described as delamination of the alumina film with a simultaneous formation of flakes and a rough topology. Some assumption about the origins of these effects are speculated below.

ALD Al_2O_3 is highly conformal. Nevertheless, there still is some small variation of density in the deposited film. The reason for this is that the ALD uses gaseous precursors and the ordering of the deposited atoms during each half-cycle is probabilistic. Therefore, the regions with different atomic ordering are generated on sub-nanometre scale. Thus, the flakes observed in the SEM images (shown in Section 4.2) can be a result of this variation of the atomic ordering. Presumably, some nanometre size regions in the bulk of the films are more favourably ordered and remain intact during the DIW treatment, while the boundaries of such regions have less stable atomic ordering, which means weaker bonds with the surrounding atoms resulting in breaking of these bonds during the treatment. The variation of the atomic ordering is enhanced by the hydrogen and carbon residuals originating from the ALD precursors. The intact pieces of alumina delaminate and form the observed flakes.

The grass-like topology of the surface is presumably generated while drying the sample. After the immersion the samples were taken out of water and dried in the air under a nitrogen flow from a nitrogen gun. Water has high surface tension: 78.2 dyn/cm at 20°C compared to, for example, benzene with 28.8 dyn/cm at the same temperature [26]. This affects the topology making the surface of the alumina film to collapse into the peaks observed in the SEM images (Section 4.2). This effect is most well seen while studying the surface of the films treated at lower temperatures (Figure 4.6).

Raman spectroscopy measurements were performed on the ALD alumina

film before and after the DIW treatment, but they didn't show any noticeable changes in the Raman spectra. X-ray diffraction measurement also failed to show any difference in porous alumina before and after annealing (the annealing procedure was mentioned in Section 4.2 and was not a part of the ARC fabrication). It is also challenging to use these techniques as the thicknesses of the as-deposited Al_2O_3 are small, and thick films can not be processed by the DIW throughout all their depth. Small structural changes in thin films are very challenging to detect. Other characterization methods, like Fourier transform infrared spectroscopy, can be used for further study of the DIW treatment, but were not performed by the author, as this work concentrates on the usage of porous alumina as an ARC.

4.4 Transmittance measurements

Transmittance spectra of the glass samples coated with porous alumina were obtained in an *Agilent Cary 7000* spectrometer. Performance of the coatings fabricated at various DIW temperatures was examined at angles of incidence spanning from 0° to 80°. The studied wavelength range of the transmitted light was 350 – 800 nm.

The fabricated porous alumina coatings increase transmittance by two approaches explained in Section 2.3: index matching and destructive interference. This means that both the refractive index and the thickness of the film affect the overall transmittance spectrum. In addition, the transmittance peak in the spectrum strongly depends on the thickness of the film (see Equation 2.13).

From Figure 4.9 it can be seen that alumina coatings processed at temperatures higher than T_{cr} increase the transmittance from ~92% to ~95%. This enhancement in the transmittance is broadband, it affects approximately equally all the studied wavelengths in the 350 nm – 800 nm range. The coating fabricated at 48.2°C slightly decreases the transmittance because it has refractive index of 1.446, while the optimal refractive index for the soda-lime glass is

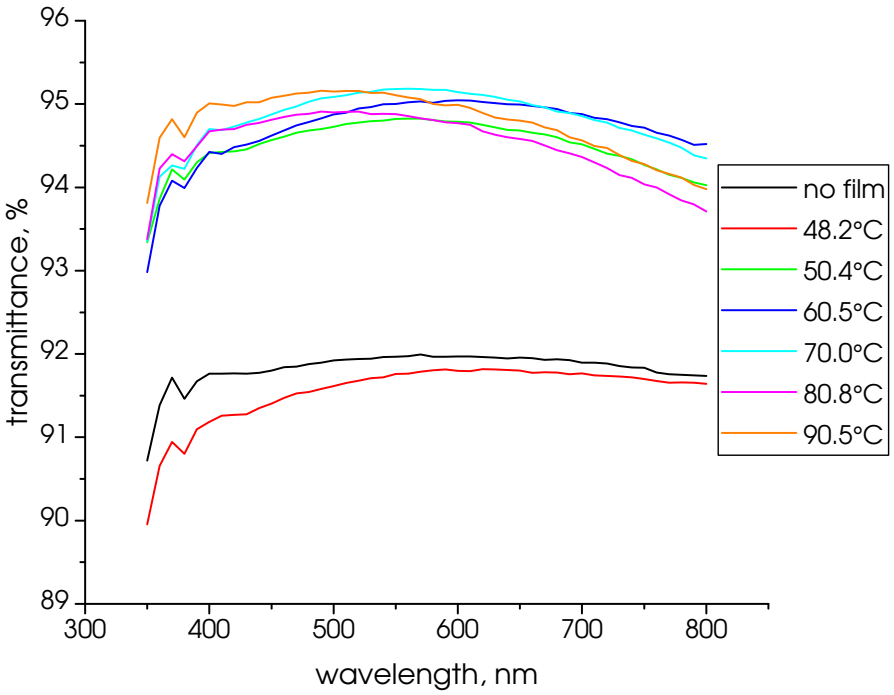

Figure 4.9. Zero incidence angle transmittance spectra of single-side coated glass samples with the porous alumina DIW treated at different temperatures. The black line indicates the transmittance spectrum of a non-coated glass.

1.23 (see Subsection 2.3.1).[3] The best performance is achieved in the coatings fabricated at 70°C and 90.5°C. Overall, the dependence of the transmittance from the temperature of the DIW processing is rather complex, because both refractive index and the resulting film thickness change with the conditions of the treatment.

According to Equation 2.13 the peaks in transmittance for the coating fabricated at 70°C and 90.5°C should be obtained at 602 nm and 585 nm, respectively. However, the peaks are shifted from their theoretical position to the shorter wavelengths, as can be seen from Figure 4.9. This relates to the fact that the coatings have a gradient refractive index profile and the destructive interference conditions are more complex than for a film with a constant index across its profile.

[3]The refractive indexes of the fabricated coatings are listed in Table 4.1.

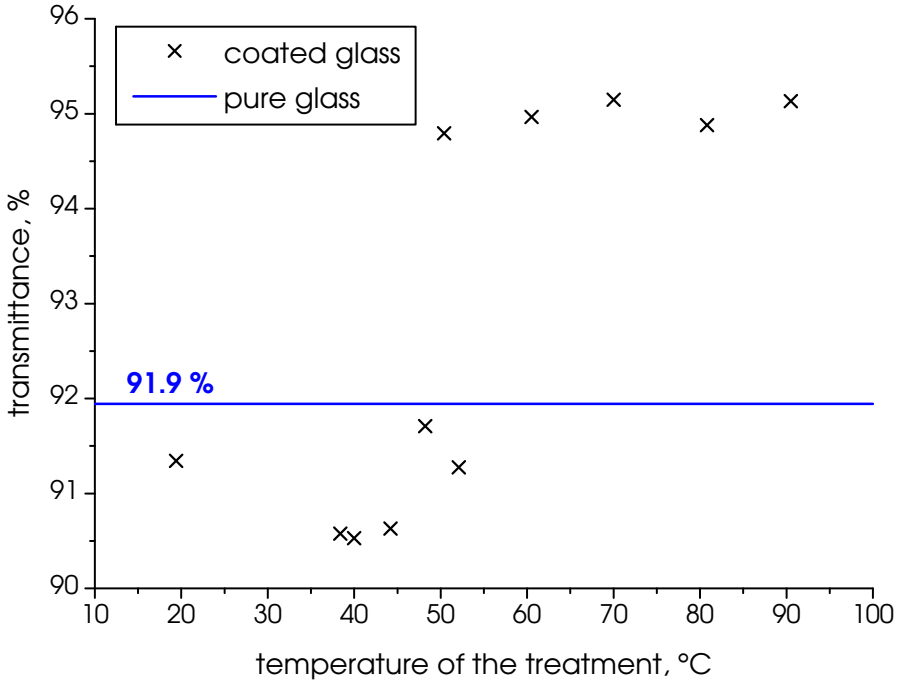

Figure 4.10. Dependence of the zero incident angle transmittance of the glass samples coated with DIW treated alumina on the temperature of the DIW processing. Transmittance was measured at the wavelength of 530 nm. The blue line shows the transmittance level of a non-coated glass.

Figure 4.10 shows the dependence of the transmittance of alumina coated glass samples on the temperature of the DIW treatment. It can be clearly observed that the coatings treated below T_{cr} only decrease transmittance through the glass, but the porous alumina coatings enhance the resulting transmittance by about 3%. It can be also seen that the temperature of the DIW processing does not significantly affect the performance of the film as long as it is higher than T_{cr}.

The glass samples coated with the porous alumina film on both sides showed transmittance up to 99.5% for the green light (around 530 nm). The transmittance spectra for the double-side coated glass samples is presented in Figure 4.11. The film treated at 90°C shows the best performance, as its refractive index is the closest to the optimal value of 1.23 among the fabricated films (see Table 4.1 and Figure 4.1). The average transmittance across the visible range

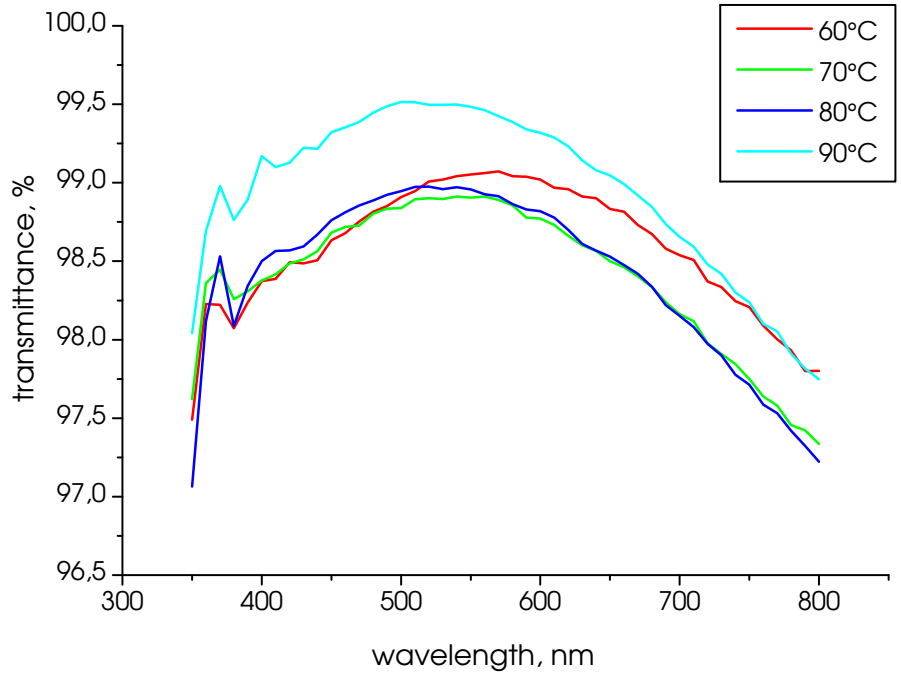

Figure 4.11. Zero incident angle transmittance spectra of glass samples double-side coated with porous alumina treated at different temperatures.

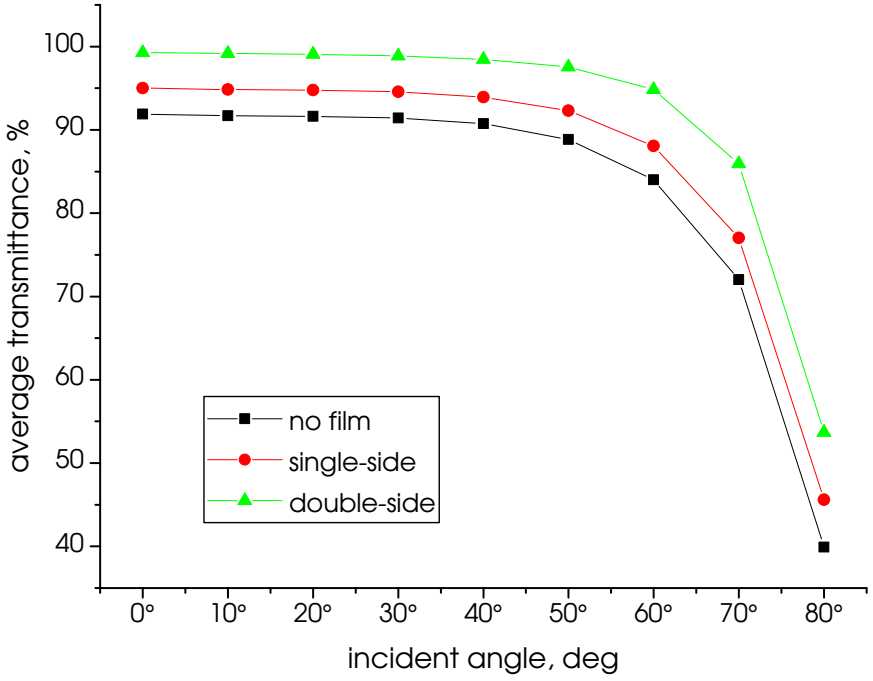

Figure 4.12. Dependence of the averaged transmittance across the visible spectrum on the incident angle of the light. The black curve indicates the values for a non-coated glass, the red curve for a single-side coated glass with alumina film (DIW treated at 90.5°C), and the green curve for a double-side coated glass (DIW treated at 90°C).

of the light spectrum (from 400 nm to 680 nm) is 99.3% with the lowest value of 98.9%.

The porous alumina film also shows good performance at high incident angles, keeping transmittance at the level of 94.8% at 60° incidence of the light for a double side coated glass (as shown in Figure 4.12). The enhancement in the transmittance is not independent on the angle of incidence, but gives better results at high incident angles: at 0° incidence the observed increase in the transmittance due to the double-side coating is 7.4%, but at 70° incidence the same film increases transmittance by 13.9% compared to the non-coated glass.

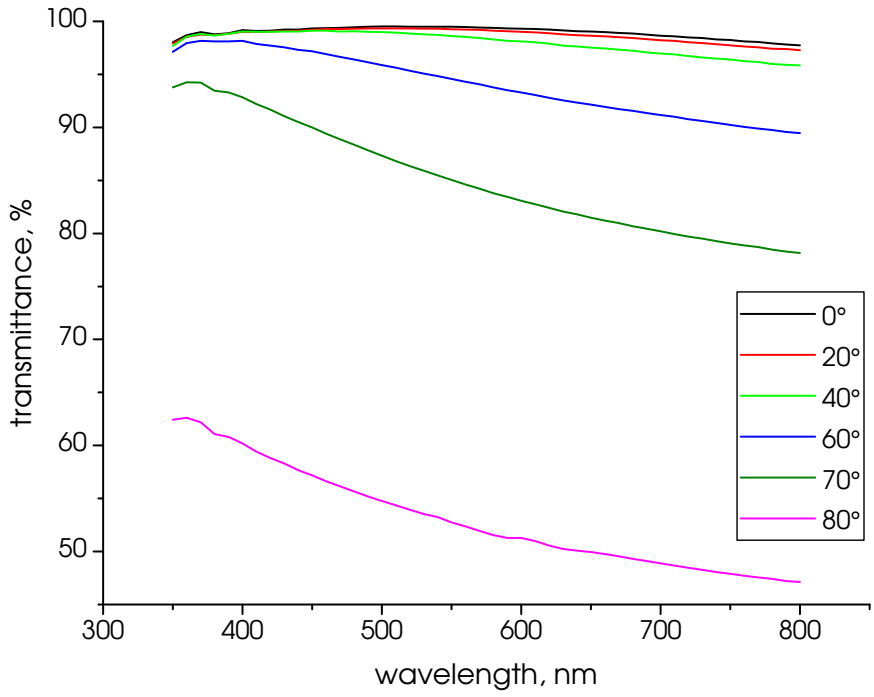

Figure 4.13. Transmittance spectra of the double-side coated glass (treated at 90°C) at different incident angles.

Figure 4.13 demonstrates transmittance spectra of the double-side coated glass at different incident angles. It can be seen that transmittance at the longer wavelengths decreases more significantly with the increase of the incident angle. This phenomenon affects the colour reproduction of the coated glass at

high incident angles.

Chapter 5

Summary

In this work anti-reflective coatings were fabricated from nanoporous alumina. The coatings were created in two steps: first alumina was deposited on soda-lime glass by ALD and secondly deposited films were immersed into heated deionized water for 30 min at various water temperatures spanning from room temperature to 90°C. Single- and double-side coated glass samples were prepared. The result of the treatment temperature on the structure and properties of the alumina film was investigated and transmittance spectra of the coatings were obtained.

It was shown that DIW processing transforms ALD alumina into a nanoporous state with the treatment temperature of ~50% (critical temperature T_{cr}) or higher. This transformation is accompanied with a drop in the effective refractive index from 1.64 (as deposited) film to 1.17 – 1.20 for nanoporous alumina. In addition, increase in the film thickness was observed. Refractive index and thickness were measured by ellipsometry. According to the thickness and refractive index changes in the alumina film the porosity levels of the coatings were calculated with the help of the effective medium theory by three different methods. The results well correlated qualitatively showing porosity of $70\% - 80\%$ in the films processed at temperatures beyond T_{cr}.

SEM images were obtained for the visual demonstration of the structure and showed a rough, grass-like topology of the nanoporous alumina. AFM

measurements were performed to measure the roughness of the films. The dependence of the roughness on the temperature of the treatment well correlated with the effective refractive index and the film thickness behaviour. According to the SEM images the DIW treatment is believed to cause delamination of the alumina and creation of flakes, which form the nanoporous structure.

Finally, the transmittance spectra of the prepared samples were measured. The spectra were obtained for the wavelength range of $350 - 800$ nm at incident angles varying from 0° to 80°. Nanoporous alumina coatings increased the transmittance through the glass in wide spectral range by ca. 3% for single-side coated samples. The DIW processing temperature had little effect on the performance as long as it was higher than T_{cr}. Double-side coatings reduced reflectance from 8% (non-coated glass) down to 0.5% at the wavelength of about 530 nm with average reflectance over visible range of spectrum of 0.7%. The increase in transmittance of the double-side coated glass at 70° light incident angle was 13.9% compared to 7.4% at normal incidence.

The new nanoporous alumina anti-reflective coatings give remarkable increase in transmittance for soda-lime glass in wide spectral range and at high incident angles. The ALD technique is capable of processing large sample areas from both sides at the same time. The DIW treatment is extremely cheap and easy to carry out and the process can be scaled to a large number of samples in a single run. Overall, the developed fabrication method of ARCs seems promising for industrial scale applications due to its low cost and efficiency. Future studies may imply increasing the wear-resistance of the coating as well as deeper understanding of the physics and chemistry behind the DIW treatment.

Bibliography

[1] Puurunen, R. L. Surface chemistry of atomic layer deposition: A case study for the trimethylaluminum/water process. *Journal of Applied Physics 97*, 12 (2005).

[2] Perros, A. C. P. *Thermal and plasma-enhanced atomic layer deposition: the study of and employment in various nanotechnology applications*. PhD thesis, Aalto University School of Electrical Engeneering, 2015.

[3] George, S. M. Atomic layer deposition: An overview. *Chemical Reviews 110*, 1 (2010), 111–131.

[4] Miikkulainen, V., Leskelä, M., Ritala, M., and Puurunen, R. L. Crystallinity of inorganic films grown by atomic layer deposition: Overview and general trends. *Journal of Applied Physics 113*, 2 (2013), 021301.

[5] Larrieu, G., and Han, X.-L. Vertical nanowire array-based field effect transistors for ultimate scaling. *Nanoscale 5* (2013), 2437–2441.

[6] Cleveland, E. R., Banerjee, P., Perez, I., Lee, S. B., and Rubloff, G. W. Profile evolution for conformal atomic layer deposition over nanotopography. *ACS Nano 4*, 8 (2010), 4637–4644.

[7] Puurunen, R. Growth per cycle in atomic layer deposition: A theoretical model. *Chemical Vapor Deposition 9*, 5 (2003), 249–257.

[8] Widjaja, Y., and Musgrave, C. B. Quantum chemical study of the mechanism of aluminum oxide atomic layer deposition. *Applied Physics Letters 80*, 18 (2002), 3304–3306.

[9] Lipson, A., Lipson, S. G., and Lipson, H. *Optical physics*. Cambridge University Press, 2010.

[10] Yoldas, B. E. Investigations of porous oxides as an antireflective coating for glass surfaces. *Appl. Opt. 19*, 9 (May 1980), 1425–1429.

[11] Raut, H. K., Ganesh, V. A., Nair, A. S., and Ramakrishna, S. Antireflective coatings: A critical, in-depth review. *Energy Environ. Sci. 4* (2011), 3779–3804.

[12] Niklasson, G. A., Granqvist, C. G., and Hunderi, O. Effective medium models for the optical properties of inhomogeneous materials. *Appl. Opt. 20*, 1 (Jan 1981), 26–30.

[13] Aspnes, D. E., Theeten, J. B., and Hottier, F. Investigation of effective-medium models of microscopic surface roughness by spectroscopic ellipsometry. *Phys. Rev. B 20* (Oct 1979), 3292–3302.

[14] Bruggeman, D. A. G. Berechnung verschiedener physikalischer Konstanten von heterogenen Substanzen. I. Dielektrizitätskonstanten und Leitfähigkeiten der Mischkörper aus isotropen Substanzen. *Annalen der Physik 416*, 8 (1935), 665–679.

[15] Yoldas, B. E., and Partlow, D. P. Formation of broad band antireflective coatings on fused silica for high power laser applications. *Thin Solid Films 129*, 1 (1985), 1–14.

[16] Yoldas, B. E. Alumina sol preparation from alkoxides. *American Ceramic Society Bulletin 54*, 3 (1975), 289–290.

[17] Yoldas, B. E. Alumina gels that form porous transparent al2o3. *Journal of Materials Science 10*, 11 (1975), 1856–1860.

[18] Chen, J., Wang, B., Yang, Y., Shi, Y., Xu, G., and Cui, P. Porous anodic alumina with low refractive index for broadband graded-index antireflection coatings. *Applied optics 51*, 28 (2012), 6839–6843.

[19] Jiang, H., Yu, K., and Wang, Y. Antireflective structures via spin casting of polymer latex. *Opt. Lett. 32*, 5 (Mar 2007), 575–577.

[20] Li, X., Gao, J., Xue, L., and Han, Y. Porous polymer films with gradient-refractive-index structure for broadband and omnidirectional antireflection coatings. *Advanced Functional Materials 20*, 2 (2010), 259–265.

[21] Robbie, K., Sit, J., and Brett, M. Advanced techniques for glancing angle deposition. *Journal of Vacuum Science & Technology B 16*, 3 (1998), 1115–1122.

[22] Kennedy, S. R., and Brett, M. J. Porous broadband antireflection coating by glancing angle deposition. *Applied optics 42*, 22 (2003), 4573–4579.

[23] Kim, L. H., Kim, K., Park, S., Jeong, Y. J., Kim, H., Chung, D. S., Kim, S. H., and Park, C. E. Al2o3/tio2 nanolaminate thin film encapsulation for organic thin film transistors via plasma-enhanced atomic layer deposition. *ACS applied materials & interfaces 6*, 9 (2014), 6731–6738.

[24] Abdulagatov, A., Yan, Y., Cooper, J., Zhang, Y., Gibbs, Z., Cavanagh, A., Yang, R., Lee, Y., and George, S. Al2o3 and tio2 atomic layer deposition on copper for water corrosion resistance. *ACS applied materials & interfaces 3*, 12 (2011), 4593–4601.

[25] Zhang, L., Jiang, H., Liu, C., Dong, J., and Chow, P. Annealing of al2o3 thin films prepared by atomic layer deposition. *Journal of Physics D: Applied Physics 40*, 12 (2007), 3707.

[26] Harkins, W. D., and Brown, F. The determination of surface tension (free surface energy), and the weight of falling drops: The surface tension of water and benzene by the capillary height method. *Journal of the American Chemical Society 41*, 4 (1919), 499–524.

Appendix A

Glass slides' specifications

The properties of the glass slides used as a substrate for anti-reflective porous alumina coating.

CORNING® 2947-75x25
Length: 75 mm
Width: 25 mm
Thickness: 0.96 to 1.06 mm
Soda Lime Glass Code No. 0215[1]:

Chemical comp.: SiO_2 73%, Na_2O 14%, CaO 7%, MgO 4%, Al_2O_3 2%

Refractive index: 1.515 @ Sodium D line

[1] http://www.tedpella.com/technote_html/0215%20corning%20glass.pdf